RESEARCH ARTICLE

Holistic Enlightening of Blackspots With Passive Tailorable Reflecting Surfaces for Efficient Urban mmWave Networks

SIMON HÄGER[ID]**, (Student Member, IEEE), KARSTEN HEIMANN**[ID]**, STEFAN BÖCKER**[ID]**, (Member, IEEE), AND CHRISTIAN WIETFELD**[ID]**, (Senior Member, IEEE)**

Communication Networks Institute (CNI), TU Dortmund University, Dortmund, 44227 North Rhine-Westphalia, Germany

Corresponding author: Simon Häger (simon.haeger@tu-dortmund.de)

ABSTRACT Mitigating outage regions is of particular interest for emerging millimeter-wave (mmWave) and future sub-terahertz frequency cellular networks. Whereas smart radio environments based on metasurfaces constitute a key concept for 6G research, current networks cannot be served as new control procedures are required. Although small prototypes are already emerging, costs will be higher for the dense deployment of reconfigurable intelligent surfaces (RISs) compared to passive reflectors. It is argued that passive reflectors can be used to effectively, cost-efficiently, and permanently boost connectivity in well-defined service areas. Leveraging the advantages of 3D printing and spray-painted conductive varnish, we introduce the Holistic Enlightening of bLackspots with passIve reflectOr moduleS (HELIOS) approach which is characterized by its scalability and parametrizability to meet the reflection requirements derived from sophisticated network planning. These slim reflectors meet the core criteria of ease of installation and minimal visual impact on the cityscape, which are imperative for market success. Our measurement-based comparison of prototypes against typical metal/aluminum reflectors shows at least equal reflectivity at a higher practicality of the proposed manufacturing process. The conducted simulation study validates the modular reflector pattern design process and finds a trade-off between the reflector efficiency and the minimum protrusion depth, which relates to the number of modules in the designated mounting area. An urban ray-tracing simulation-based case study further underlines the high applicability of the proposed approach, with the growth of the beyond line-of-sight (LOS) connectivity region being nearly twice as large for a site-tailored heterogeneous HELIOS configuration than that for a simple reflector plate.

INDEX TERMS Millimeter-wave, passive reflector, beyond line-of-sight connectivity, additive manufacturing.

I. INTRODUCTION

5G and beyond networks are expanding to the mmWave and sub-THz domains to offload the sub-6 GHz spectrum, thus cushioning the exponential growth of cellular network traffic [1]. This move also enables modern use cases, such as extended reality (XR) applications, cooperative automated driving, and high-accuracy positioning. Although the radio environment at mmWave frequencies offers large bandwidths, it has been considered hostile

The associate editor coordinating the review of this manuscript and approving it for publication was Mohammad S. Khan[ID].

owing to increased path losses until a paradigm shift occurred in the last decade. The additional losses can be compensated for by introducing large-scale antenna arrays and beamforming transceivers. On the downside, reduced obstacle penetration, increased absorption, and reduced diffraction nonetheless reduce the effective coverage area of mmWave base stations (BSs) compared to traditional sub-6 GHz cells [2]. As a result, there will be numerous outage regions, so-called blackspots, which would be too expensive to develop with additional sites. Therefore, it is difficult to achieve robust mobile cellular mmWave connectivity.
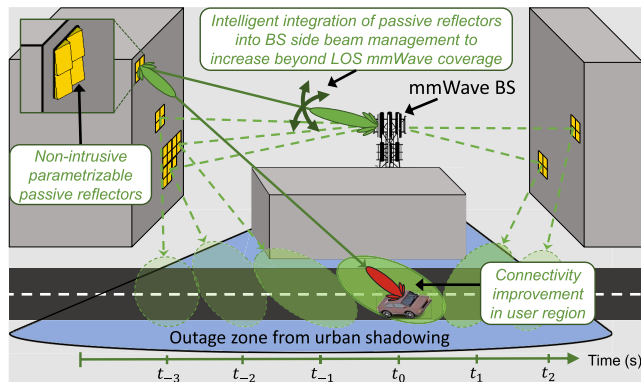
FIGURE 1. Bringing seamless mmWave connectivity to users in urban shadows using large-scale deployments of cost-efficient passive reflectors with conductive coated surfaces. Practicality is ensured via intelligent network planning enabling the customization of slim modular, easily mountable geometries and the integration of passive reflectors into the BS's beam management.

In the context of the ongoing discussions on 6G, research is investigating RISs to dynamically reflect impinging electromagnetic (EM) waves in the desired direction, as needed [3]. Simulation results in [4] indicate strong benefits for vehicular mmWave connectivity. And thus, network coverage can be extended, both outdoors and indoors, in a more cost-efficient and sustainable way than when deploying additional BSs [3], as also recognized by the European Telecommunications Standards Institute (ETSI) [5]. However, dynamically reconfigurable metamaterials are still at an early stage and will be rather expensive against non-reconfigurable, passive reflectors considering the envisioned and required large-scale reflective surface areas. Moreover, the adaptability of the reflection imposes new beam management and channel estimation challenges adding to the existing difficulties of maintaining in-coverage and beyond LOS mmWave links throughout both user and ambient mobility [6].

Typically, network operators rely on sophisticated network planning such that areas of interest are served with the desired signal quality [7]. This planning process may incorporate reflecting surfaces to extend the coverage permanently, for example, when a cell needs to be extended around a street corner to also cover the intersecting street. Whereas simple reflectors may be sufficient to solve this problem, RIS technology offers additional improvements in terms of the coverage of dynamic shadow regions, such as those obstructed by a truck passing by. When using passive, non-reconfigurable reflectors, the temporary occurrence of shadowed areas must be considered in advance during the operator's network planning to provide the required illumination for such cases. We argue that static reflectors address the fundamental needs of network operators, as they are aware of the outage regions and can therefore design and deploy custom reflectors to enlighten the blackspots.

Our concept assumes that sophisticated network planning-based information about the reflector's exact mounting position allows the BS to ideally align the antenna beam towards the reflector. Furthermore, with information about the reflection characteristics and the corresponding coverage region, the entirely passive reflectors can be incorporated intelligently into the network side beam management: If the user moves into a shadow region, the BS beam switches from the LOS propagation path to the reflector-based path. Further, as illustrated in Fig. 1, the BS can also switch its beam to a different reflector if the user roams deeper into the shadow region that is covered by several reflectors, each serving a well-defined area. Thus, through network planning that determines the number and configuration of non-reconfigurable, passive reflectors, similar improvements in coverage can be achieved as with a RIS, even if it requires more wall space. Nonetheless, as illustrated in this work, expenses will be lower, while design and deployment flexibility can be maintained: We show that 3D printing enables the prototyping of custom geometries and thus provides suitable reflection patterns, whereas a subsequent conductive coating enables high reflectivity.

Our HELIOS concept allows for piecewise and simplified mounting, and particularly, neither intrudes on the cityscape nor requires any power supply in order to reduce the inhibition level against mounting of these passive reflectors on various properties. See Fig. 1 for an illustration of the reflector geometry which is forced to exhibit a very low protrusion by design. Considering the proposed manufacturing process depicted in Fig. 2, which is discussed in detail in Sec. III, passive reflector installations could moreover be integrated smoothly into multi-functional facades, for example by merging with vertical gardening/photovoltaic installations or thermal/noise insulation. Beyond extending and improving coverage for pedestrians and motor vehicles on the ground, they may also be used to serve aerial vehicles in the future, e.g., for parcel deliveries [8]. Accounting for the traditional downtilt installations of cellular network antennas and the limited array field of view, passive reflectors can efficiently extend the coverage area of the network operator on the ground and in the air.

Against this background, the main contributions of this manuscript are as follows.

- We compare and discuss the different available options to extend mobile radio network coverage.
- This work introduces a sophisticated design and manufacturing process for the prototyping of the proposed HELIOS reflectors, which constitute a purely passive solution providing enhanced network coverage according to the operator's requirements.
- We explore the close links between network planning, reflector design, and intelligent integration into the network operation.
- The HELIOS concept is validated through extensive laboratory mmWave measurements as well as simulations, which are also evaluated scaled to an urban case study.

The remainder of this paper is structured as follows: Referring to related work, Sec. II provides a brief overview

of the current state of research within the field of mmWave reflecting surfaces. Sec. III elaborates on the multi-stage design and manufacturing process of HELIOS reflectors. After evaluating the proposed concept in Sec. IV by means of measurements and simulations, we conduct an urban case study in Sec. V. Last, Sec. VI concludes this work with a summary of our findings and an outlook on future work.

II. METHODS FOR EXTENDING MOBILE RADIO NETWORK COVERAGE TO BLACKSPOTS

There is a vast interest in the development of RIS technology, which is also referred to as intelligent reflecting surfaces (IRSs). They typically consist of a planar array of so-called unit cells with the RIS's overall far-field reflection characteristic arising from the superposition of the individual cells' reflections. These depend on each unit cell's reflection phase shift and amplitude which are tunable in real-time by a controller [3], [27]. The authors in [28] examine the attained reflection patterns when using either digital phase shifters, limited by the number of bits, or analog ones. Either way, the RIS can optimize its reflection using suitable inputs, e.g., concerning the angle of reflection or beamwidth. As such, they can be efficiently used to turn a non-line-of-sight (NLOS) link into multiple LOS links [14]. In the literature, the term RIS typically indicates a (nearly) passive realization, although active variants for signal amplifications are also under investigation [29]. Implementation aspects for the two types are surveyed in both [30] and the references provided in the respective columns in Table 1. In the following sections, we use the term RIS for the passive RIS flavor.

As discussed in Sec. I and summarized in Table 1, RISs have numerous advantages over additional BSs, e.g., in terms of cost-efficiency, sustainability, and applicability to any radio environment. Moreover, RIS technology is the enabler for so-called smart radio environments as follows. Whereas RISs can boost connectivity by focused reflections, they may also limit electromagnetic field exposure (EMFE), e.g., at playgrounds, by broad reflections distributing power more equally in the coverage area or redirecting the incident EM wave entirely [31]. In the latter case, depending on the RIS size, NLOS-based EMFE may be suppressed significantly in target regions due to the exhibited absorption-like behavior. Moreover, unlike when using active components, passive reflecting surfaces are not expected to create severe EMFE, but naturally regulatory constraints must always be upheld. These features are also key to increasing the secrecy of communication, as demonstrated in [32], or decreasing inter-cell interference in certain areas. Lastly, they can be seamlessly integrated into various sensing services in the scope of 6G joint communication and sensing (JCAS) and,

TABLE 1. Assessment of coverage enhancement approaches, as evolved from the traditional deployment of BSs, based on referenced comparative works.

Metrics Categories/Features	Extra BS	Relay	Repeater	RIS/IRS Active	RIS/IRS Passive	Passive Reflector Proposed HELIOS Concept	Passive Reflector Mechanical Steerable Surface	Passive Reflector Simple Plate/Foil
Power Consumption								
Full Stack	●	○	○	○	○	○	○	○
Decoding/Channel Estimation	●	●	◐	◐	○	○	○	○
Amplification	●	●	●	●	○	○	○	○
Steering (Electronical or Mechanical)	●	◐	◐	●	●	○	●	○
Control Link	◐	◐	◐	●	●	○	●	○
None/Passive	○	○	○	○	○	●	○	●
Coverage Type								
New Cell	●	○	○	○	○	○	○	○
Active Antennas	●	●	●	●	○	○	○	○
Generalized Snell's Law of Reflection [9]	○	○	○	●	●	◐	○	○
Snell's Natural Law of Reflection	○	○	○	◐	◐	●	●	●
Signal Forwarding								
Full Stack	●	○	○	○	○	○	○	○
Decode & Forward	◐	●	○	○	○	○	○	○
Amplify & Forward	○	○	●	●	○	○	○	○
Real-time Control of Reflection	○	○	○	●	●	○	●	○
None/Predefined	○	○	○	○	○	●	○	●
Control								
Backhaul (Wired or Wireless)	●	●	●	○	○	○	○	○
Control Signaling	●	◐	◐	●	●	○	●	○
None/Predefined	○	◐	◐	○	○	●	○	●
Material and Equipment								
Radio Unit (Transmit and/or Receive)	●	●	◐	◐	○	○	○	○
Active Antennas	●	●	●	●	○	○	○	○
Passive Antennas	○	○	○	◐	●	◐	○	○
Metamaterial	○	○	○	●	●	◐	◐	○
Tailorable Reflection	○	○	○	●	●	●	●	○
Reflective Material	○	○	○	●	●	●	●	●
Deployment								
Rooftop/Pole Mount	●	●	●	○	○	●	●	○
Wall/Ceiling Mount	●	●	●	●	●	●	●	●
Arbitrary Surface	○	○	○	●	●	◐	○	●
References	[10–12]	[12–18]	[14–18]	[6, 15–20]	[6, 14–19, 21, 22]	*This Work*	[6, 19, 22, 23]	[6, 18, 24–26]

Feature Classification: ● – Typical feature. ◐ – Applies in selected realizations or system states. ○ – Does not apply.

(a) Network planning and reflector parametrization aided by simulations.

(b) Prototype production process with 3D printing and conductive coating. Subsequent piecewise mounting of modules.

(c) Lab and field validation of various target reflection characteristics.
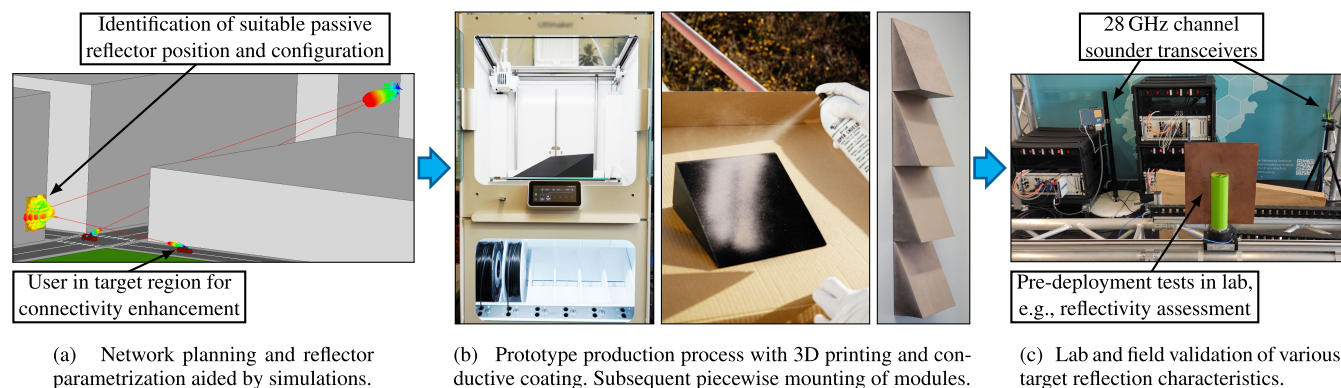
FIGURE 2. End-to-end design and scalable low-cost manufacturing process for scenario-tailored HELIOS deployments.

therefore, e.g., improve positioning service availability and quality [31].

Due to the promising advantages of RISs for wireless communications, various channel models like for example [33] have already been derived and are widely recognized in the research community. Using this model, we have previously verified that mobile/vehicular mmWave communications may indeed profit significantly from the presence of such link opportunities [4]. Even more so if the reflection gain is increased further by scaling the footprint of the RIS [33], [34]. Using several reflectors with optimized deployment, it has further been shown that even a less dense mmWave site deployment becomes feasible, even when using simpler non-reconfigurable passive reflectors [35]. Whereas these can also be deployed in the scope of 6G-enabled sensing services, as shown in [36], passive reflectors are typically considered for communication-centric purposes in the literature due to their simplistic set of features compared to other approaches, cf. Table 1.

However, RISs are in their infancy with the first prototypes having emerged recently, e.g., in [27] and [37]. In the meantime, alternatives, as presented in [38], actively amplify and redirect the incident wave in certain directions in a relay/repeater-like fashion. In contrast, the authors in [39] present a (fully) passive reflector solution not capable of adjusting the reflection angle dynamically. Nonetheless, by removing the real-time reconfigurability, the passive reflector is expected to result in lower costs than RISs and relays/repeaters [14], e.g., due to the lack of hardware for the control link, steering, amplification, decoding, and channel estimation, cf. Table 1. Therefore, they come with better scalability of reflecting surface installations, i.e., in numbers and/or size. For this reason, the design developed in [39] follows the low-cost prototype presented in [40]. The costs may only be lowered further by removing the need for dipoles and special substrates as enabled by our proposed approach. Moreover, whereas the passive reflector in [39] exhibits a narrow beam, diffuse reflectors have already been proposed in the literature [41], [42]. Whereas the previous works do not consider multi-beam capabilities as illustrated in [43], this

could be achieved by combining two differently configured passive reflectors. This illustrates that passive reflectors can still be tailored to the network operator's requirements. In addition, passive reflectors, contrary to RISs, require no control link as well as neither a power supply nor a battery. As the challenge of mmWave beam management remains unaffected, passive reflectors are compatible with 5G networks.

In this work, we present a new design and manufacturing process for scalable passive reflectors which have several advantages against the deployment of new BS sites and the previously discussed reflector types, cf. Table 1, in particular simple integration into the network, low cost, and scalability in terms of numbers and size. In literature, passive reflectors such as metal plates [26] and aluminum foil wrapped pillars [25] have recently been studied within urban environments. In both cases, measurements have validated an increase of multipath richness and higher receive power. However, both reflectors are not suitable for strategic outdoor deployments: Foil wrinkles, whereas metal-based reflectors are expensive. Further, the mounting determines the reflection angle, as illustrated in [35], thus increases expenses due to mounting complexity while also reducing the robustness against wind and weather. Moreover, such a mounting is intrusive to the cityscape and thus unlikely to be adopted. Therefore, we formulate the following *requirements for passive reflectors* permanently extending and enhancing the network coverage into preconfigured directions:

1) Reflecting surface, possibly with non-conductive base.
2) Parametrizability, e.g., reflection angle and beamwidth in azimuth and elevation domain.
3) Low protrusion for non-intrusiveness.
4) Simple mounting and assembly of large reflector areas.

III. FROM NETWORK PLANNING TO ROLLOUTS: ENGINEERING CUSTOM PASSIVE REFLECTORS

In the following section we present our combined approach of designing, manufacturing, testing, and deploying passive reflectors tailored to specific urban scenarios as illustrated

in Fig. 2. Sec. III-A focuses on the additive manufacturing-based production process, whereas Sec. III-B presents the overall passive reflector's geometry based on a simulation-aided modular design process.

A. PASSIVE REFLECTOR MANUFACTURING CONCEPT

In essence, a reflector primarily consists of a reflective surface of a suitable shape such that a predetermined reflection pattern is imposed on impinging waves. All other parts of the reflector geometry are overhead, but are for instance required for mounting and robustness. A solid metal reflector would therefore be a waste of resources due to excessive material overhead. Moreover, bringing metal into the right form is expensive in terms of required plant and equipment. Therefore, the idea to use aluminum foil as proposed in [25] and [44] in order to add reflectivity to a non-metal geometry has its merits. However, for the reasons described in Sec. II, the feasibility of this solution is limited particularly when considering elaborate reflector surface shapes.

In this work, we propose a multi-stage design and manufacturing process capable of generating appropriate reflector geometries and embedding the intended reflection surface with high reflectivity characteristics: Starting from a simplified model of the general reflection geometry, ray-tracing based EM simulation studies are conducted to cater for the individual reflection conditions and the conception of the designated reflector module as sketched in Fig. 2a. By means of 3D printing technology, any possible reflector module geometry is produced with little effort. Using a low infill density, the material overhead is minimized. For our prototype prints, we have used 3D printers with polylactic acid (PLA)[1] plastic filament at a fine layer height (< 0.1 mm) as well as a gradual infill strategy with an overall density of less than 10% [45]. In a second production step, as exemplified in [46] for the manufacturing of an antenna array, a conductive coating is applied to the reflector surface in order to generate metal-like reflection characteristics. Instead of galvanization, we propose to spray-paint the conductive coating, e.g., using silver-coated copper [47], to reduce the complexity for the rapid prototyping.

Overall, the described manufacturing process, as depicted in Fig. 2b, facilitates a rapid and economic prototyping, since all components are available off-the-shelf at reasonable prizes and simple to handle. Whereas the experimental evaluations of the produced reflectors are conducted by means of our mmWave experimental platform [48] utilizing channel sounder measurements, field trials are left for future work. Despite manufacturing only small numbers for this initial work, the scalability for industrial production with high quality requirements and subsequent mass deployment is generally feasible and may profit from economy of scales

---

[1]Other commercially available filaments, e.g., PETG, can be used for outdoor deployments in regions with high temperatures and high UV intensity.
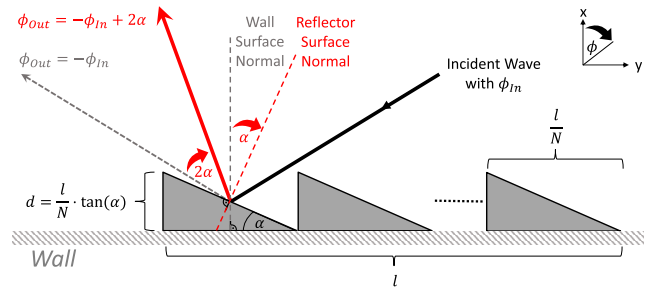

FIGURE 3. HELIOS concept: Modules with reflecting surface reflect impinging wavefront with azimuth angle ϕ_{In} depending on slope angle $\alpha > 0°$, $\alpha \in \mathbb{R}$, towards desired reflection angle ϕ_{Out}. The deployment is further characterized by the number of modules $N \gg 1$, $N \in \mathbb{N}$, within a large wall footprint of length l affecting the protrusion depth d.

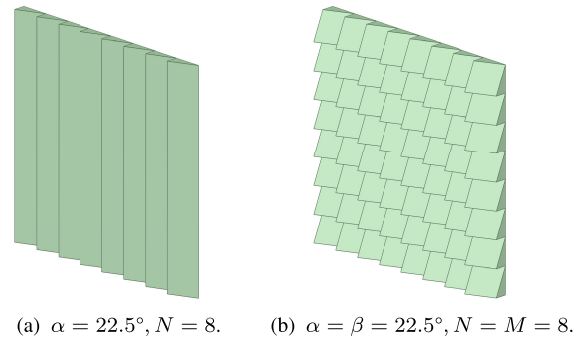(a) $\alpha = 22.5°$, $N = 8$.   (b) $\alpha = \beta = 22.5°$, $N = M = 8$.

FIGURE 4. CAD polyhedrons for 3D printing with square footprint ($l_y \times l_z$): Adapting HELIOS from (a) only manipulating the azimuth reflection angle ϕ_{Out}, cf. Fig. 3, towards (b) additional tuning of the elevation angle θ_{Out}. (l_y, α, N) and (l_z, β, M) are parametrized to match the requirements from network planning before tiling-like mounting.

considering similar/repeated urban deployment scenarios, e.g., at crossroads.

B. DESIGN OF NON-INTRUSIVE PASSIVE REFLECTORS

Following the law of reflection, passive reflectors need to be custom-tailored regarding the incident wave angle from the well-aligned BS beam and the desired angle of reflection based on network planning-based requirements, cf. Fig. 1. As a consequence, the reflector surface normal vector must point right between these two angles. Our solution approach HELIOS closes this gap as follows: Using a modular sawtooth-like shape as illustrated in Fig. 3, the protrusion depth of such a frontage-mount reflector is reduced proportionally to the number of modules N, thus facilitating an unintrusive deployment. Another benefit of large N is a decrease of material consumption, as the overall reflector volume is proportional to $1/N^2$. HELIOS is easily extended such that the reflection angle may also be tuned in elevation, cf. Fig. 4. Regardless of the parametrization of the used modular reflectors, e.g., (α, l, N), the mounting of large reflector surface areas within the cityscape will resemble the process of tiling a wall using tile glue/cement. As such, even small footprint production facilities are feasible for use as the overall reflector may be manufactured and put together piecewise. We note that the spray-painting of the conductive
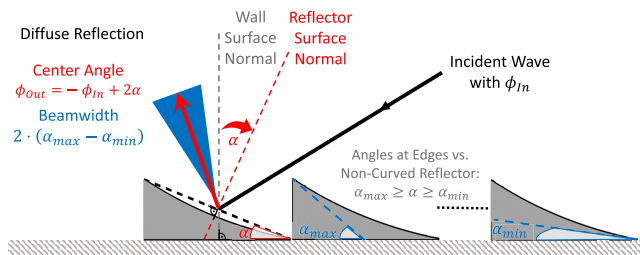
FIGURE 5. HELIOS using modules with sophisticated shapes to realize broader beams by integrating a concave curvature, e.g., a section of a circular arc. Further modifications such as gaps between the modules or limiting the curvature to the non-shadowed areas of the modules are omitted for brevity.
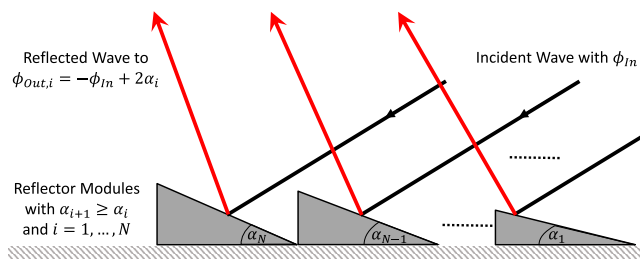

FIGURE 6. HELIOS employing different types of modules in the overall constellation to create a broad reflection beam. In the far field of the passive reflector deployment each module will serve an individual direction, thus achieving a diffuse reflection.

coating could even be done after installation on a property facade.

We note that a similar design of repeated modules has already been contemplated in [41] with the requirements of being *periodic, symmetric, parametrizable*, but was discarded due to self-shadowing-based inefficiency. This decision was not based on a detailed study and made despite proposing the option that $N - 1$ gaps could be introduced between the HELIOS modules. Moreover, the work did not consider our requirements on low depth and simple mountability, which we discussed previously. In [49] a blazed grating-based approach similar to this work is approximated, however, the arising overall shape loses the sawtooth-like form and consists of controllable pistons with sub-wavelength protrusion. The ensuing mechanical RIS [49] is not sufficiently scalable to large footprints, but provides interesting starting points for future optimization of this work's HELIOS module shapes.

We point out that the authors in [41] have illustrated that broader beams may be generated in a parametrizable way by adding concave or convex features to the module surfaces in Fig. 3. A similar idea has also been put forward in [44] but considering the use of reflectors in the very near field of the BS; in [50] the idea is applied for broadening of both azimuth and elevation reflection characteristics. We use this as a starting point to address parametrizable HELIOS reflection beamwidths as follows. Considering a planar EM wave impinging on each reflector module, a diffuse reflection may be achieved when the surface is not flat. For example, a section from a circle embedded into the previously proposed reflector achieves a uniformly distributed reflection beam as

depicted in Fig. 5. This is because each reflector module exhibits the continuous range of slope angles from $\alpha_{\min}$ to $\alpha_{\max}$. In case the outermost slope angles are selected symmetrically around the center angle α from Fig. 3, the infinitesimal specular reflections of the arc constitute a width of $2(\alpha_{\max} - \alpha_{\min})$ symmetrically split around target angle $\phi_{\text{Out}} = -\phi_{\text{In}} + 2\alpha$. Accounting for the deployment of several nearby modules, the curvature could also only be embedded into the upper part of the baseline triangle-like reflector shape depicted in Fig. 3 such that reflections in the direction of $-\phi_{\text{In}} + 2\alpha_{\min}$ are not affected by self-shadowing.

In this work we further outline an alternative method to adapt the HELIOS reflection pattern using a discrete set of differently shaped reflector modules as depicted in Fig. 6. The figure shows that each of the N modules reflects in a predetermined direction with slopes $\alpha_1 \leq \alpha_2 \leq \cdots \leq \alpha_N$ such that a broad beam may be recreated in the far field of the passive reflector constellation, i.e., beyond the focal point of the reflected EM waves. However, this also requires a careful selection of the $\alpha_i, i = 1, \ldots, N$, slopes such that no notch appears in the reflection pattern. This process could be implemented iteratively using simulations as illustrated by the first stage in Fig. 2. The slopes can also be selected such that two or more distinct reflection angles are targeted. Moreover, curved modules, i.e., sections of a circle or parabola, are also compatible to this HELIOS flavor, as discussed before. As illustrated by Fig. 4, both azimuth and elevation reflection characteristics can be optimized. It must further be noted that the previously discussed heterogeneous designs may also be adapted for mounting at non-flat walls, e.g., columns, as well as on poles. The combination with different patches of entirely passive metamaterials represents another interesting development perspective.

We have therefore shown numerous mutually compatible methods to design the HELIOS reflection pattern according to the operator's requirements from the mmWave network planning stage. The design process for the shape and positioning of the HELIOS reflectors must take into account the targeted illumination areas as well as regulatory limits and rules for EMFE.

C. OUTLINE OF KEY EVALUATION SECTIONS
The proposed HELIOS concept from Secs. III-A and III-B is evaluated within the Secs. IV and V. Table 2 points out the key sections together with a classification of the data basis.

TABLE 2. Overview of the evaluation sections in this paper.

Sec.	Title	Data Basis
IV-C1	Validation of the Conductive Coating	measurements
IV-C2	On the Far-field Characteristics of Modular Reflectors	simulations
V-B	Eval. of Passive Reflector-based mmWave Coverage Enhancements	simulations

IV. EVALUATION OF PROPOSED PASSIVE REFLECTOR DESIGNS AND MANUFACTURING PROCESS
In this section, sample reflectors, as introduced in Sec. IV-A, are evaluated and compared to metal and aluminum foil based
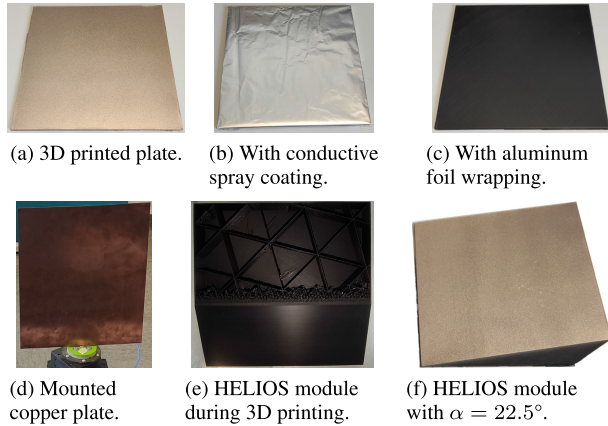
(a) 3D printed plate. (b) With conductive spray coating. (c) With aluminum foil wrapping.

(d) Mounted copper plate. (e) HELIOS module during 3D printing. (f) HELIOS module with $\alpha = 22.5°$.

FIGURE 7. Surfaces *(a)–(d)* under test for their reflectivity with aluminum foil and copper serving as a reference. Sample HELIOS module during 3D printing *(e)* and finally after coating the designated surface *(f)*.

reflectors. After explaining the measurement and simulation methodology in Sec. IV-B, the results are finally discussed in Sec. IV-C.

A. PASSIVE REFLECTORS

Following the process outlined in Sec. III, we have manufactured several passive reflectors. The footprint of the individual reflector modules is 18.3×18.3 cm. In order to assess the spray-paint coating and its manufacturing process, we have created 3D-printed PLA plates with a thickness of 3 mm as shown in Figs. 7a to 7c. In comparison, a 25×31 cm copper plate with a thickness of less than 1 mm (cf. Fig. 7d) and a household-typical, commercial-off-the-shelf aluminum foil with a µm-range thickness (cf. Fig. 7c), which is similar to the conductive coating (2 layers) [47] in Fig. 7b, are used. We have further printed several HELIOS modules with $\alpha = 22.5°$ for various experiments. These are thus capable of changing the azimuth reflection angle by 45°. By means of Fig. 7e we give a brief insight into the preceding material and cost efficient prototype manufacturing process using a variable infill density. Fig. 7f shows the final passive reflector module prototype (3D print with applied conductive silver-coated copper spray coating) which can be included in the proposed large-scale HELIOS reflector constellations, cf. Sec. III.
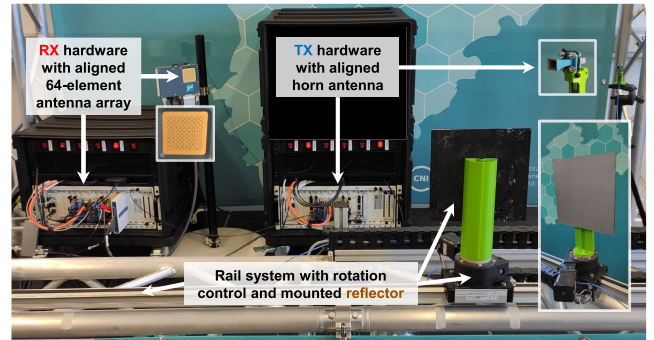
B. EXPERIMENTAL AND SIMULATION SETUPS
1) METHODOLOGY OF REFLECTOR MEASUREMENTS

The manufactured reflectors are evaluated via measurements using a mmWave transceiver system [51]. We summarize the details of the setup in Table 3 along with further technical details from [52] and [42] on the channel sounder measurements. An in-depth discussion of the channel sounder mode operating principle can be found in [52]. Earlier works have used the system to assess the reflection characteristic of copper plates at various frequencies. In recent work, reflector-based radio channels have been measured at different carrier frequencies with the system using azimuth beam sweeping

(a) Sketch of the laboratory setup in top view.

(b) Photo of reflectivity study of a spray coated PLA plate, cf. Fig. 7b.

FIGURE 8. Channel sounder measurement setup with RX beam sweeping.

on the transmitter (TX) and receiver (RX) sides, cf. [42]. In contrast, we have extended the capabilities of the channel sounder to support RX side azimuth and elevation beam sweeping at several hundreds of beambook entries per second using a phased-array antenna [53]. This is reasonable because of the network planning step of the proposed design process, due to which the BS transmission beam orientation is already known and the corresponding alignment is achieved during installation. A horn antenna is installed on the TX side to avoid RX oversaturation at short distances [54]. As in our previous work [48], we operate the mmWave transceiver system at 28 GHz which belongs to the 5G band n257. A bandwidth of about 1.5 GHz is used for the channel measurements as such bandwidths are supported in 5G via carrier aggregation (CA) and enable ultra-high data rates [55].

The experimental lab setup is illustrated in Fig. 8a, in which it is shown that the passive reflector is installed on our rail system as presented in [48], thus allowing both linear movements and rotations of the reflector in a reproducible manner. For the setting $\xi = 1.7$ m and $\gamma = 0°$, we have validated the orientations of the antennas with a laser pointer, e.g., when mounted to the horn antenna, the point of light after copper-plate reflection was perceptible in the middle of the antenna array panel, and vice versa. The complete laboratory measurement setup is shown in Fig. 8b: Due to the central transceiver rack the LOS path from TX (right) to RX (left) is blocked intentionally.

Before the measurements, we calibrated the system such that the non-ideal hardware response is equalized, cf. [52]. Moreover, the time measurements have been calibrated for the reflector-based NLOS propagation path length of

TABLE 3. Details about the mmWave laboratory measurement setup [52].

Parameter	Description/Value
TX Antenna Type	horn antenna (10.0 dBi gain, 54.4° HPBW)
RX Antenna Type	planar 8×8 phased-array
RX Beam Sweeping	16,341 pencil beam orientations with $\phi, \theta \in [-60°, 60°]$ in steps of 1°
Beam Switch Interval	2 ms (32.7 s per RX beam sweep)
mmWave Carrier Frequency	28 GHz (5G band n257)
Intermediate Frequency (IF)	13.5 GHz (to/from remote radio head (RRH))
Effective Bandwidth	1.536 GHz: 2,048 subcarriers, 750 kHz spacing
Channel Sounder Waveform	root-raised cosine (RRC) filtered sequence
I/Q Transmit Sequence	2,048 bit Zadoff-Chu sequence
Measurement Aggregation	32 repetitions
Analog/Digital Converter (ADC)	3.072 GS/s sampling rate
CIR Time Resolution and Span	$\Delta\tau = 0.65$ ns, $\tau_{max} = 1.33$ µs
Reflectors Under Test incl. Width (W) and Height (H)	copper plate (W = 25.0 cm, H = 31.0 cm)
	aluminum foil wrapped PLA plate (W, H = 18.3 cm)
	conductive spray painted PLA plate (W, H = 18.3 cm)

FIGURE 9. Two dimensional RX beam sweeping-based channel measurements. Whereas the non-coated PLA plate suffers from poor reflections, the proposed coated PLA plate achieves considerable path loss reductions.

2.91 m. For the subsequent evaluation of the acquired measurement data in this work, we limit our investigation to the measured path loss in decibels (dB) for brevity. Using RX side beam sweeping with azimuth and elevation angles $\varphi, \theta \in [-60°, 60°]$ in steps of 1°, each sweep captures 16,341 channel impulse responses (CIRs). Based on these extensive measurements, the proposed printed reflector plate with conductive varnish is compared to copper and aluminum reflectors.

2) METHODOLOGY OF REFLECTOR PATTERN SIMULATIONS

The experimental measurements are complemented with EM simulations using the shooting and bouncing ray (SBR+) solver of the Ansys Electronics software framework [56]. This tool allows for simulation of directional mmWave channels as used in [57] and illustrated by Fig. 2a emulating the measurement setup. It has also been used to study the scattered near field of a RIS prototype in a small, well-defined area [27]. However, to account for urban deployment scenarios, we instead use the tool to simulate the far-field reflection patterns of passive reflectors similar to Meng et al. [43] in terms of a scalability analysis, as the distance between infrastructure-mounted reflector and transceiver is typically much larger than in our laboratory setup. In Fig. 2a we depict such a sample urban deployment with a frontage-mounted 32×32 HELIOS reflector structure and the according simulated far-field pattern. Due to investigating long range characteristics, we employ a 28 GHz planar wavefront source with incident angles $(\phi_{In}, \theta_{In}) = (33.1°, 0°)$ mirroring the measurement setup.

Against this background, the scaled simulations are first compared to the plate measurements with different rotations γ, thus examining the gains of RXs misaligned to the reflector main lobe by $\Delta\phi_{Refl.} = 2\gamma$, see Fig. 8a. The simulative analysis considers the *total power gain* which is the ratio of reflected energy into a given direction over the incident wave energy. This is a distance-normalized metric of the simulator as the gain would otherwise be negative infinity for the infinite far field.
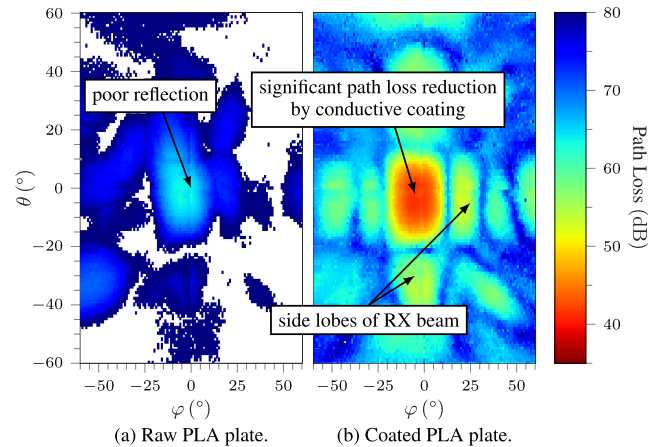
This methodology is afterwards applied to three 2×2 HELIOS constellations consisting of 18.3×18.3 cm elements as follows: The first setup uses the same four elements with $\alpha = 22.5°$ for a narrow reflection, whereas the subsequent ones target broader reflections. In the second approach, four identical but curved elements are used with $\alpha_{min} = 19.5°$ and $\alpha_{max} = 25.5°$. The third reflector constellation, in contrast, leverages four different elements with slope angles $(\alpha_1, \alpha_2, \alpha_3, \alpha_4) = (19.5°, 21.5°, 23.5°, 25.5°)$, as depicted in Fig. 11 together with the results.

Moreover, we conduct a sensitivity analysis in which the far-field patterns of HELIOS reflectors ($\alpha = 22.5°$) with different numbers of modules N, but overall constrained to the same footprint, are investigated along their azimuth and elevation angles in the range of $-90°$ to $90°$ with 0.25° angular granularity, respectively. Note that with $\gamma = -\alpha$ the compound reflector is aligned with the TX and RX positions, since the assumed divergence α from the frontage orientation is compensated by the rotation γ for the setups geometry.

C. RESULTS AND DISCUSSION

1) VALIDATION OF THE CONDUCTIVE COATING

As initial proof-of-concept, Fig. 9 verifies the considerable path loss reduction by means of conductive coating compared to the raw PLA. With a perfect RX beam alignment, the path loss is reduced by up to 20 dB (for this reflector size). Also the half-power beamwidth (HPBW) related alignment tolerance can be observed as well as the beamforming-typical sidelobes. Moreover, the reflector allows for a higher probability of successful signal detection and decoding, even with totally misaligned RX beams. This may also facilitate beam management procedures of 5G and beyond mobile networks, since a perfect alignment may not be required for the reception of initial signaling information. Our measurements have therefore confirmed that the 3D printed, spray-painted passive reflectors indeed increase both the channel quality and the number of spatial link opportunities.
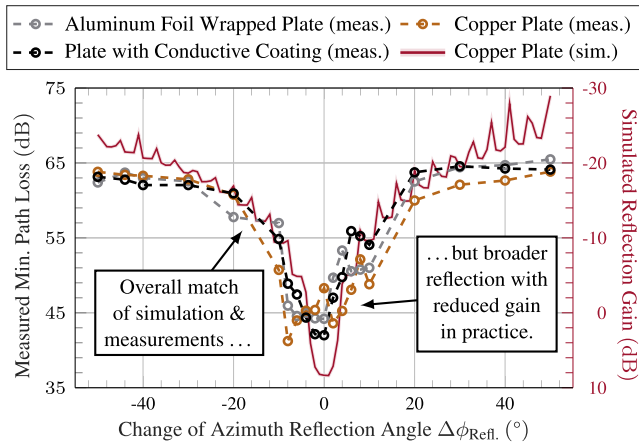
FIGURE 10. Minimum measured path loss for reflector plates with different (surface) materials for varying rotation angles $\gamma \in [-25°, 25°]$. Simulated far-field gains of a rotable copper plate towards RX validate the measurements.
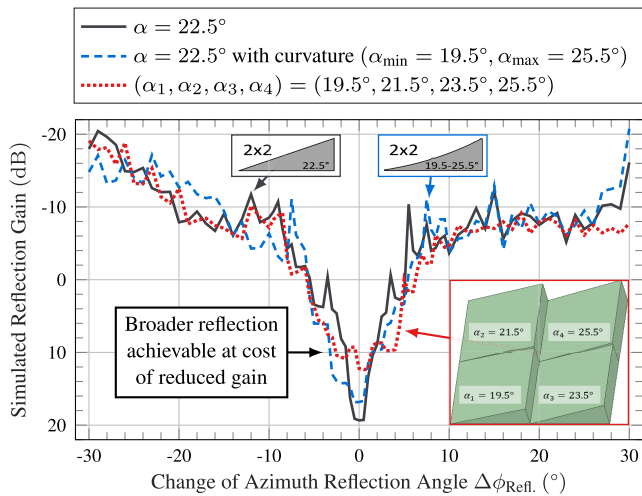

FIGURE 11. Moving from a single reflector element to constellations of multiple reflectors. Far-field reflection gain of 2×2 HELIOS reflector variations with (18.3×18.3 cm footprint per module as in Fig. 10). With the slope angle α being 22.5°, $\gamma \in [-52.5°, 7.5°]$ such that the reflector main lobe misalignment $\Delta\phi_{\text{Refl.}}$ towards the UE at $\phi_{\text{Out}} = 33.1°$ is in the depicted range.

TABLE 4. Characterization of reflection patterns from Fig. 11 in terms of gain and two beamwidth metrics.

Description of 2×2 HELIOS Constellation	Max. Gain	3 dB/10 dB Beamwidth
$\alpha = 22.5°$	19.3 dB	1.75°/ 3.25°
$\alpha = 22.5°$, 19.5°–25.5° curvature	16.8 dB	3.25°/ 6.25°
$\alpha_k = 19.5° + (k-1) \cdot 2°, k \in \{1,2,3,4\}$	12.4 dB	6.50°/10.25°

The reflection characteristics of the different materials are compared in Fig. 10. The gains of the proposed conductive coating are about 2 dB–3 dB larger than for the aluminum plate, however, the angular domain of reasonable orientation remains similar. This could be due to a higher conductivity of the silver-coated copper paint [47] or due to wrinkles in the aluminum foil, with either case being an advantage of the proposed manufacturing approach over the one from [25]. The copper plate, despite its larger size, comes

with a more pronounced, up to 6.3 dB degradation of the minimum measured path losses. This is slightly higher than the observed path loss deviations of at most 4 dB between a copper plate and a pre-commercial passive reflector for different mmWave carrier frequencies in [42]. The reason for this could be the excessive copper plate weight in contrast to the used thinness, which results in a slight bending of the plate as copper is malleable. The effect leads to an observable broader reflection. Passive copper reflectors therefore either need thick plates for compensation (at higher expenses due to increased material overhead) or need an inner body around which the copper surface is applied to keep it in form. This is not suitable for complex reflector geometries.

2) ON THE FAR-FIELD CHARACTERISTICS OF MODULAR REFLECTORS

The narrow distribution of reflection power seen in Fig. 10 is suitable for stationary settings such as for wireless fronthaul and fixed-wireless access (FWA). However, it is impractical for real deployments with mobile users, particularly because the reflection angle cannot be changed after installation. Therefore, as also noted in [39], passive reflectors with broader beams are required, which can be achieved HELIOS via more complex module geometries and/or constellations of different modules. Thus, we briefly investigate the feasibility of our proposed concepts for the creation of broader reflections using three different 2×2 reflector constellations. Each of them is designed with a center slope of $\alpha = 22.5°$ with two of them being designed to produce 12° reflection beams using the concepts depicted in Figs. 5 and 6, respectively. Due to the focal length of the proposed reflectors, we do not expect our previous laboratory measurement setup to be able to capture the broadening effect of the reflection. Thus, we continue to use the far-field simulation methodology which was previously confirmed by measurements.

Compared to before, the overall footprint in the simulations is 36.6×36.6 cm, i.e., doubled in either dimension. As a consequence, we identify increased reflection gains in Fig. 11. Moreover, the simulated far-field reflection patterns underline that broader beams can indeed be achieved at the cost of a reduced maximum reflection gain. Table 4 summarizes the key metrics of the considered reflectors. It can be seen that the 10 dB beamwidth of the reflection is near the expected value, whereas the HPBW (3 dB beamwidth) is restricted to a smaller angular region. With further already outlined HELIOS optimization steps, such as introducing gaps between the reflectors, the main reflection lobe could be broadened, particularly for the curved reflectors.

By means of scalable simulations, the far-field reflection patterns of thin, easily mountable HELIOS reflectors are evaluated for several numbers of modules N as shown in Fig. 12. When increasing N and proportionally reducing the reflector depth d, the reflector pattern becomes more irregular with stronger sidelobes along the azimuth dimension ϕ. This originates from the edges of the modules which result in

(a) $N = 1$, $d = 15.1$ cm. (b) $N = 2$, $d = 7.6$ cm. (c) $N = 4$, $d = 3.8$ cm. (d) $N = 8$, $d = 1.9$ cm.
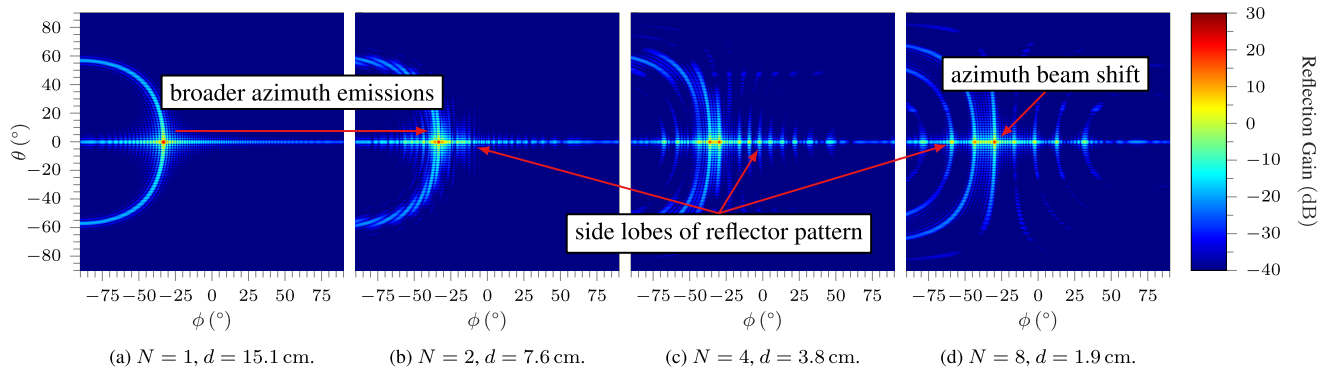
FIGURE 12. Sensitivity analysis of thin HELIOS reflectors reveals trade-off between achievable protrusion and target reflection characteristics, which can be mitigated by the proposed EM simulation-aided design stage: Simulated far-field pattern of unintrusive reflectors for different N with a fixed overall square footprint $l = 36.6$ cm. Used rotation $\gamma = -22.5°$ compensates slope $\alpha = 22.5°$. Compared to (a), increasing N results in undesired sidelobes due to wedge diffraction. In (c), the reflector depth is already smaller than typical corrugated metal facades. For extreme case (d) a main reflection lobe shift is observed as wedge diffraction becomes dominant because the effective reflection area per module approaches λ. Due to the very small considered footprint l and sufficiently low achieved protrusions d, $N > 8$ is not depicted.

diffraction around the protruding corners. In addition, the reflection gain decreases with increased N, since shadowing reduces the effectively utilizable surface area. Considering typical protrusions d of several centimeter for common urban corrugated metal facades, selection of $N \in [2, 4]$ suffices for a non-intrusive deployment. For comparison, the relay/repeater-like mmWave reflector prototype studied in [38] also comes with a depth of 3.4 cm.

For the extreme case $N = 8$ (given the small reflector footprint) in Fig. 12d, we further observe a deviation of the main lobe reflection angle, thus efficiency diminishes. This shows that the number of modules N cannot be increased arbitrarily, and thus, the protrusion of the reflector has a lower bound based on, e.g., the footprint size. However, since edge diffraction becomes overly dominant, this is expected. Moreover, with the effective surface area per module approaching the wavelength λ, undesired scattering-like reflection characteristics appear. As a consequence, it is underlined that our proposed ray-tracing assisted reflector geometry design stage in Fig. 2 is needed to validate the conformance of particularly thin reflector patterns (e.g., sub-1 cm protrusion to match other prototypes as studied in [37], [39], [49], and [32]) with design requirements (e.g., main reflection beam orientation, beamwidth, etc.). As we showed that there is a good match between real reflection behavior and far-field pattern simulations, cf. Fig. 10, the reflection pattern may then be optimized by, e.g., readjusting the slope angles and module spacings, see Sec. III.

V. CASE STUDY: PASSIVE REFLECTORS FOR ENHANCED URBAN mmWave CONNECTIVITY

In this section we conduct a simulative case study comparing the mmWave connectivity gains in a NLOS street canyon provided from different passive reflectors. Sec. V-A introduces the urban scenario, the reflectors, and the modeling of the link budget. Afterward, Sec. V-B evaluates the UE side receive power gains over the whole scenario as well as the distributions of path loss.

TABLE 5. Key details about the urban street corner simulation scenario.

Parameter	Description/Value
BS Position (x, y, z)	(309.9 m, 170.1 m, 10.0 m)
BS Antenna Type	8 × 8 uniform planar array (UPA) with 12.0° HPBW
BS Beam Orientation (ϕ, θ)	(170.17°, −2.46°)
Reflector Footprint Center (x, y, z)	(195.0 m, 170.0 m, 5.0 m)
Reflector Footprint Size $(x \times z)$	3.0 m × 3.0 m
Considered Reflector Scenarios	4 different reflectors vs. baseline
UE Position Grid Center (x, y, z)	(180.0 m, 180.0 m, 1.5 m)
UE Position Grid Size $(x \times y)$	120.0 m × 120.0 m
UE Position Grid Density $(\Delta x, \Delta y)$	uniform 1 m spacings
UE Antenna Type	omni-directional
mmWave Cell	28.0 GHz carrier (5G n257 band) using 100 MHz bandwidth
Link Budget	144 dB (40.0 dBm to −84.0 dBm)

A. PASSIVE REFLECTORS FOR URBAN SCENARIO

We investigate the practical applicability of the proposed unintrusive passive reflectors in an urban scenario which is depicted in Fig. 13. We summarize key details on the scenario in Table 5 along with further details that are discussed in the following paragraphs. The ray-tracing simulations were conducted with the previously presented simulation tool, again considering a 28 GHz carrier. The BS is mounted at a height of 10 m at the corner of a 100×100×20 m building and leverages an idealized pencil beam pattern with a beamwidth of 12°, thereby mirroring our commercial 8 × 8 UPA. The BS beam is directed at the center of the designated 3 × 3 m mounting area for the passive reflectors ($\phi_{In} = 80.17°$, $\theta_{In} = 2.46°$). The center-point of the reflector footprint is 5 m from the street corner at a height of 5 m. In the simulations we use copper as the material for the reflecting surfaces whereas the buildings and streets are assumed to be made of concrete, parametrized according to [58]. Along the street corner area, channels between BS and several thousand of UEs are simulated with the UEs being uniformly distributed in a 1 m-spaced grid up to 60 m from the intersection at a height of 1.5 m. The UEs use omni-directional antennas in order to avoid ambiguity due to the leveraged beam patterns and beambooks.
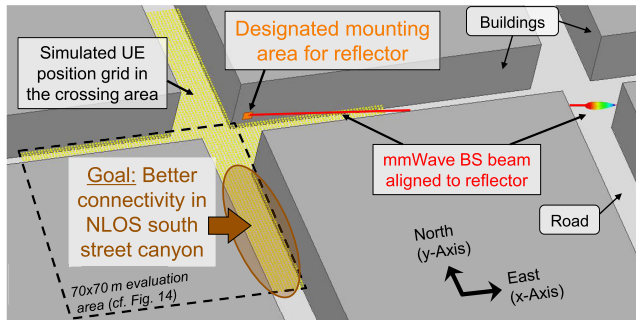
FIGURE 13. Example simulation scenario in which the mmWave cell's coverage is to be extended around a street corner into the shadowed street canyon at the bottom.

Overall, we consider four reflector deployments which are compared to the *baseline scenario* in which no passive reflector is used. We illustrate three of them, i.e., the intrusively mounted copper plate and the two slim HELIOS reflector variations, in Fig. 14 together with the results.

- *Flat copper plate*: Flat metallic surface covers designated wall section. The reflection angle is not modified.
- *Intrusive copper plate*: Metallic plate is mounted at designated section of building wall such that the impinging EM wave is reflected into the south corridor ($\alpha = 27.6°$, $\phi_{Out} = -25°$). The deployment is overly intrusive to the cityscape with $d = 156.8$ cm.
- *HELIOS reflector (narrow beam)*: $N = 32$ elements with slope angles $\alpha_1, \ldots, \alpha_{32} = 27.6°$ mirroring the above reflector, but with a non-intrusive depth of just 5 cm.
- *HELIOS reflector (broad beam)*: Based on reflection pattern simulation feedback we deploy a tailored passive reflector attaining a broader beam. The deployed modules are configured from a discrete set of seven slope angles assigned to the 32 modules as follows.

  1) $\alpha_{32}, \ldots, \alpha_{29} = 32.6°$ 2) $\alpha_{28}, \ldots, \alpha_{24} = 30.1°$
  3) $\alpha_{23}, \ldots, \alpha_{18} = 27.6°$ 4) $\alpha_{17}, \ldots, \alpha_{12} = 25.1°$
  5) $\alpha_{11}, \ldots, \alpha_{7} = 22.6°$ 6) $\alpha_{6}, \ldots, \alpha_{3} = 20.1°$
  7) $\alpha_{2}, \alpha_{1} = 17.6°$

  Thus, the maximum protrusion is 6 cm, but the target azimuth reflection angle ϕ_{Out} is in the range from about $[-15°, -45°]$ which is tailored to the whole opening of the south street canyon.

We note that the two HELIOS constellations could be modified further for an increased efficiency, e.g., elevation reflection angle and width, gaps between modules, and curved reflecting surfaces. Further, multiple reflectors could be deployed near the street crossing, potentially in series. However, this is beyond the scope of this case study as we aim to validate the practical feasibility of the HELIOS reflector using the fundamental aspects of the proposed concept.

The comparison between the baseline mmWave coverage and the four reflector-aided connectivity maps consists of two parts. On the one hand, we investigate the absolute UE side receive power differences between the reflector-enhanced and baseline scenarios. The arising empirical cumulative

distribution functions (ECDFs) of path loss in the west and south street canyons is studied on the other hand. In this context, the tolerable path loss, i.e., the link budget, is assumed to be 144 dB given an equivalent isotropically radiated power (EIRP) of 40 dBm, a UE side antenna gain of 20 dBi, and a receiver sensitivity of −84 dBm [59] using a 5G mmWave typical component carrier bandwidth of 100 MHz [55]. This corresponds to the typical link budgets in the literature, cf. [60].

B. EVALUATION OF PASSIVE REFLECTOR-BASED mmWave COVERAGE ENHANCEMENTS

We now begin to study the applicability of the proposed non-intrusive reflectors with a focus on the evaluation area outlined in Fig. 13. In Fig. 14a the absolute receive power change between the baseline scenario (mmWave network without reflector) and a reflector plate-based scenario with intrusive protrusion and mounting is depicted for the west and south street corridors. There are two problems with this solution: First, the copper plate has a protrusion of more than 1.5 m, thus even requiring a robust and durable mounting system. This solution will impose on the cityscape and is unlikely to be adopted in real-world urban mmWave networks. Second, whereas promising power gains can be seen, these are limited to a small region of the south street canyon only. As a side note, it can also be observed that the impact on the EMFE in the west street canyon is much lower. The receive power based on this BS transmit beam orientation is actually lower than before, therefore illustrating that passive reflectors decrease EMFE in non-target regions or may be used deliberately to do so in a target region.

Moving on to Fig. 14b, the protrusion is reduced to 5 cm by the HELIOS approach, which is about 3.2 % of the copper plate setup. Further, it can be seen in the figure that this solution can also bring similar high power gains of up to 60 dB at some UE positions. This shows that the concerns about self-shadowing-based inefficiencies stated in [41] do not play a major role in large-scale reflector deployments. Taking a closer look at the coverage region, a positive impact of the reflection sidelobes due to reflections of diffracted incident waves, studied in Fig. 12, can be identified as the slim modular reflector leads to an inherently greater coverage area than the intrusive plate-based approach. Nonetheless, this setup cannot serve the whole south street width due to the use of 32 identical modules with $\alpha = 27.6°$ still resulting in a rather narrow reflection. On a further note, whereas the sidelobes of the HELIOS reflector are helpful in this deployment scenario, undesired EMFE could be introduced in other scenarios. In the latter case, the reflector design would need to be customized using further simulations in the scope of EMFE-aware network planning.

We now consider the deployment of an enhanced scenario-tailored HELIOS solution with increased reflection beamwidth by using seven different types of modules with slope angles in the range of 17.6° to 32.6°, thus increasing
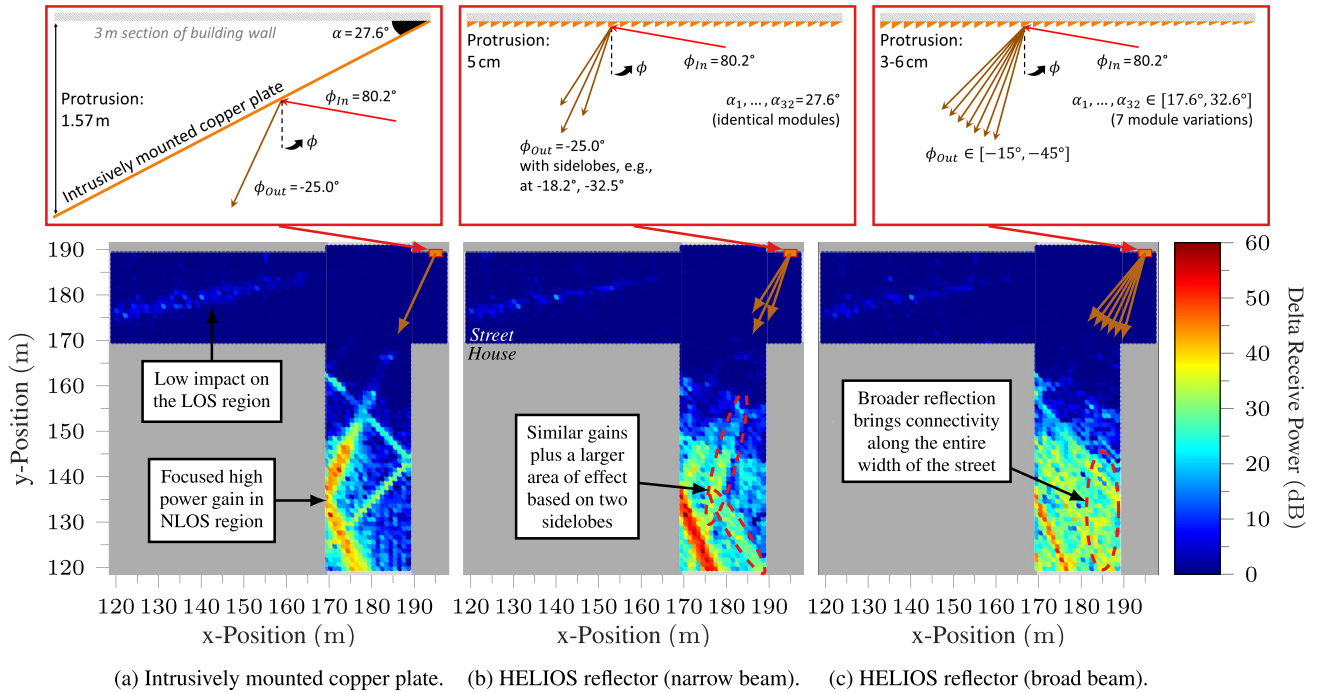
FIGURE 14. Heatmaps visualize the absolute path loss difference between reflector-based and baseline network connectivity from a bird's eye perspective: (a) Intrusive copper plate, and (b)–(c) slim HELIOS reflectors with narrow and broad reflection configuration. It can be seen that the proposed passive reflectors can indeed improve the connectivity in the target region with minimal impact on the cityscape. In a further optimization steps, the elevation angle of the reflection could be altered according to Fig. 4 to bring the south street connectivity enhancements closer to the crossing.

the maximum protrusion to 6 cm. The corresponding diffuse reflection has the following effects as shown in Fig. 14b. Whereas less UEs are served with the maximum receive power gains, a much larger overall coverage along the southern street is achieved with typical gains in the range of 30 dB to 40 dB. We have therefore shown that the proposed reflectors can indeed provide increased signal strength in the whole considered urban shadow region. Nonetheless, there are further optimization potentials which were not considered in this case study for brevity. For example, the reflection-based gains could be brought closer to the crossing if reflector elements with additional tuning of the elevation slope are used, see Sec. III-B for details.

Last, we consider the distributions of path loss for the baseline and the four reflector-based scenarios, as shown in Fig. 15. Comparing the ECDFs of the baseline scenario and the scenario in which a copper plate was mounted without any protrusion, there is little change. This underlines the importance of proper redirecting of the incident EM wave into the target region. Changing the mounting of the plate such that it becomes intrusive (1.57 m) but redirects the energy towards the target region, we find that the path loss distribution is shifted significantly. The number of outage UE positions in the shadowed south street canyon, initially 83.6 % for the baseline deployment scenario, is reduced by 25.5 percentage points to 58.1 %. With the slim, narrow beam HELIOS reflector setup even less outage positions remain (49.0 %), thus exceeding the gains of the intrusive setup by
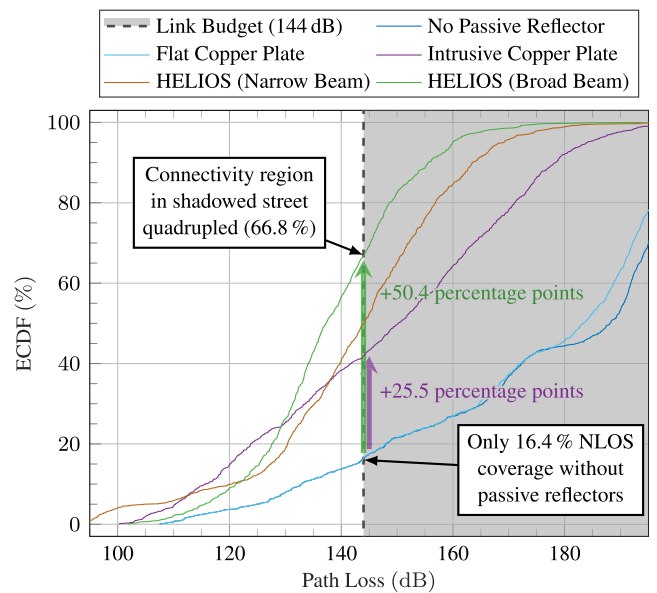

FIGURE 15. Empirical distribution of incurred path loss in predominantly NLOS south street canyon (20 x 50 m area) with and without passive reflectors. Increase in cell coverage by tailored HELIOS nearly twice that by intrusive plate.

9.1 percentage points. This is due to the arising sidelobes of the periodic modular constellation of passive reflector elements. The last approach, HELIOS with configuration for a broader reflection, deliberately exploits these effects and reduces the empirical outage probability to 33.2 %

which is much smaller than the baseline situation (83.6 %). Considering the gains in connectivity, the intrusive copper plate increased the coverage by 25.5 percentage points, whereas the tailored HELIOS comes with a change of 50.4 percentage points, cf. lengths of the purple and green arrows in Fig. 15. This shows that our proposed passive reflector is 97.7 % more effective, thus bringing connectivity into a much larger region than the classical passive reflector plate. Overall, the connectivity in the shadowed street has quadrupled using our approach. We have therefore shown with this work that the proposed HELIOS reflectors provide a parametrizable, non-intrusive method to boost mmWave connectivity in NLOS regions at low cost.

VI. CONCLUSION

In this work, we proposed HELIOS which is a comprehensive and scalable passive reflector-based concept to enhance mmWave network coverage. Using modular parametrizable reflectors, the radio environment is enhanced and enriched permanently in predetermined areas. Thus, it constitutes a green and sustainable alternative to the deployment of additional BSs. Compared to RISs, HELIOS is compatible with current radio networks as there is no need for adaptation of network operation, e.g., for additional signaling.

On the one hand, we introduced a new design and manufacturing methodology combining 3D printing and spray-paint conductive coating, which enables the material and cost-efficient production of elaborate passive reflector geometries. Using our laboratory setup, we validated the high reflectivity of the manufactured prototypes. On the other hand, we outlined the need for easily mountable and low-protruding reflectors to increase the applicability of comprehensive passive reflector deployments. We illustrated what such geometries could look like to change both azimuth and elevation reflection angles, and how they can be tuned to attain diffuse reflections. By studying the simulated far-field reflection patterns, we showed that the reflector depth cannot be reduced arbitrarily owing to shadowing and that diffraction may lead to undesired pattern characteristics. Nonetheless, a sufficiently low protrusion can be achieved without severe effects. For the design of very slim reflectors, we outlined geometry adjustments that need to be coupled with simulation feedback. Finally, with an urban case study, we further underlined the high applicability of HELIOS reflectors to enhance connectivity within a street canyon.

In future work, we aim to verify the proposed modular reflector configurations with measurements in a real mmWave network deployment. Moreover, the creation and evaluation of a HELIOS reflector-based channel model which can assist in semi-automated network planning and optimization processes is ongoing.

REFERENCES

[1] Ericsson AB. *Ericsson Mobility Report November 2022*. Accessed: Apr. 13, 2023. [Online]. Available: http://www.ericsson.com/en/reports-and-papers/mobility-report/reports/november-2022

[2] T. S. Rappaport, R. W. Heath, R. C. Daniels, and J. N. Murdock, *Millimeter Wave Wireless Communications*, 1st ed. London, U.K.: Pearson, Sep. 2014.

[3] Q. Wu and R. Zhang, "Towards smart and reconfigurable environment: Intelligent reflecting surface aided wireless network," *IEEE Commun. Mag.*, vol. 58, no. 1, pp. 106–112, Jan. 2020, doi: 10.1109/MCOM.001.1900107.

[4] K. Heimann, B. Sliwa, M. Patchou, and C. Wietfeld, "Modeling and simulation of reconfigurable intelligent surfaces for hybrid aerial and ground-based vehicular communications," in *Proc. 24th Int. ACM Conf. Modeling, Anal. Simulation Wireless Mobile Syst.*, Nov. 2021, pp. 67–74, doi: 10.1145/3479239.3485700.

[5] ETSI. *New Group on Reconfigurable Intelligent Surfaces*. Accessed: Apr. 13, 2023. [Online]. Available: http://www.etsi.org/committee?id=1979

[6] Q. Wu, S. Zhang, B. Zheng, C. You, and R. Zhang, "Intelligent reflecting surface-aided wireless communications: A tutorial," *IEEE Trans. Commun.*, vol. 69, no. 5, pp. 3313–3351, May 2021, doi: 10.1109/TCOMM.2021.3051897.

[7] C. Bektas, S. Bocker, B. Sliwa, and C. Wietfeld, "Rapid network planning of temporary private 5G networks with unsupervised machine learning," in *Proc. IEEE 94th Veh. Technol. Conf.*, Sep. 2021, pp. 1–6, doi: 10.1109/VTC2021-Fall52928.2021.9625210.

[8] M. Patchou, B. Sliwa, and C. Wietfeld, "Flying robots for safe and efficient parcel delivery within the COVID-19 pandemic," in *Proc. IEEE Int. Syst. Conf. (SysCon)*, Vancouver, BC, Canada, Apr. 2021, pp. 1–7, doi: 10.1109/SysCon48628.2021.9447142.

[9] N. Yu, P. Genevet, M. A. Kats, F. Aieta, J.-P. Tetienne, F. Capasso, and Z. Gaburro, "Light propagation with phase discontinuities: Generalized laws of reflection and refraction," *Science*, vol. 334, no. 6054, pp. 333–337, Oct. 2011, doi: 10.1126/science.1210713.

[10] A. Goldsmith, *Wireless Communications*, 1st ed. Cambridge, U.K.: Cambridge Univ. Press, Jan. 2005.

[11] E. Dahlman, S. Parkvall, and J. Sköld, *5G NR: The Next Generation Wireless Access Technology*, 2nd ed. Amsterdam, The Netherlands: Elsevier, Sep. 2020.

[12] E. Dahlman, S. Parkvall, and J. Sköld, *4G, LTE-Advanced Pro and The Road to 5G*, 3rd ed. Amsterdam, The Netherlands: Elsevier, Aug. 2016.

[13] B. Tezergil and E. Onur, "Wireless backhaul in 5G and beyond: Issues, challenges and opportunities," *IEEE Commun. Surveys Tuts.*, vol. 24, no. 4, pp. 2579–2632, 4th Quart., 2022, doi: 10.1109/COMST.2022.3203578.

[14] M. Di Renzo, K. Ntontin, J. Song, F. H. Danufane, X. Qian, F. Lazarakis, J. De Rosny, D.-T. Phan-Huy, O. Simeone, R. Zhang, M. Debbah, G. Lerosey, M. Fink, S. Tretyakov, and S. Shamai, "Reconfigurable intelligent surfaces vs. relaying: Differences, similarities, and performance comparison," *IEEE Open J. Commun. Soc.*, vol. 1, pp. 798–807, 2020, doi: 10.1109/OJCOMS.2020.3002955.

[15] Y. Liu, X. Liu, X. Mu, T. Hou, J. Xu, M. Di Renzo, and N. Al-Dhahir, "Reconfigurable intelligent surfaces: Principles and opportunities," *IEEE Commun. Surveys Tuts.*, vol. 23, no. 3, pp. 1546–1577, 3rd Quart., 2021, doi: 10.1109/COMST.2021.3077737.

[16] Z. Zhang, L. Dai, X. Chen, C. Liu, F. Yang, R. Schober, and H. V. Poor, "Active RIS vs. passive RIS: Which will prevail in 6G?" *IEEE Trans. Commun.*, vol. 71, no. 3, pp. 1707–1725, Mar. 2023, doi: 10.1109/TCOMM.2022.3231893.

[17] F. C. Okogbaa, Q. Z. Ahmed, F. A. Khan, W. B. Abbas, F. Che, S. A. R. Zaidi, and T. Alade, "Design and application of intelligent reflecting surface (IRS) for beyond 5G wireless networks: A review," *Sensors*, vol. 22, no. 7, p. 2436, 2022, doi: 10.3390/s22072436.

[18] D. Pérez-Adán, Ó. Fresnedo, J. P. González-Coma, and L. Castedo, "Intelligent reflective surfaces for wireless networks: An overview of applications, approached issues, and open problems," *Electronics*, vol. 10, no. 19, p. 2345, Sep. 2021, doi: 10.3390/electronics10192345.

[19] T. Sharma, A. Chehri, and P. Fortier, "Reconfigurable intelligent surfaces for 5G and beyond wireless communications: A comprehensive survey," *Energies*, vol. 14, no. 24, p. 8219, Dec. 2021, doi: 10.3390/en14248219.

[20] M. Alsabah, M. A. Naser, B. M. Mahmmod, S. H. Abdulhussain, M. R. Eissa, A. Al-Baidhani, N. K. Noordin, S. M. Sait, K. A. Al-Utaibi, and F. Hashim, "6G wireless communications networks: A comprehensive survey," *IEEE Access*, vol. 9, pp. 148191–148243, 2021, doi: 10.1109/ACCESS.2021.3124812.

[21] R. Alghamdi, R. Alhadrami, D. Alhothali, H. Almorad, A. Faisal, S. Helal, R. Shalabi, R. Asfour, N. Hammad, A. Shams, N. Saeed, H. Dahrouj, T. Y. Al-Naffouri, and M.-S. Alouini, "Intelligent surfaces for 6G wireless networks: A survey of optimization and performance analysis techniques," *IEEE Access*, vol. 8, pp. 202795–202818, 2020, doi: 10.1109/ACCESS.2020.3031959.

[22] P. Nayeri, F. Yang, and A. Z. Elsherbeni, "Beam-scanning reflectarray antennas: A technical overview and state of the art," *IEEE Antennas Propag. Mag.*, vol. 57, no. 4, pp. 32–47, Aug. 2015, doi: 10.1109/MAP.2015.2453883.

[23] M. Mirmozafari, Z. Zhang, M. Gao, J. Zhao, M. M. Honari, J. H. Booske, and N. Behdad, "Mechanically reconfigurable, beam-scanning reflectarray and transmitarray antennas: A review," *Appl. Sci.*, vol. 11, no. 15, p. 6890, 2021, doi: 10.3390/app11156890.

[24] J. Gomez-Ponce, N. A. Abbasi, R. Kondaveti, A. Kumar, S. Abu-Surra, G. Xu, C. Zhang, and A. F. Molisch, "Impact of common reflecting and absorbing building materials on THz multipath channels," *Radio Sci.*, vol. 57, no. 2, pp. 1–10, Feb. 2022, doi: 10.1029/2021RS007412.

[25] N. A. Abbasi, J. Gomez-Ponce, S. M. Shaikbepari, S. Rao, R. Kondaveti, S. Abu-Surra, G. Xu, C. Zhang, and A. F. Molisch, "Ultra-wideband double directional channel measurements for THz communications in urban environments," in *Proc. IEEE Int. Conf. Commun. (ICC)*, Montreal, QC, Canada, Jun. 2021, pp. 1–6, doi: 10.1109/ICC42927.2021.9500510.

[26] W. Khawaja, O. Ozdemir, Y. Yapici, F. Erden, and I. Guvenc, "Coverage enhancement for NLOS mmWave links using passive reflectors," *IEEE Open J. Commun. Soc.*, vol. 1, pp. 263–281, 2020, doi: 10.1109/OJCOMS.2020.2969751.

[27] R. Fara, P. Ratajczak, D.-T. Phan-Huy, A. Ourir, M. Di Renzo, and J. De Rosny, "A prototype of reconfigurable intelligent surface with continuous control of the reflection phase," *IEEE Wireless Commun.*, vol. 29, no. 1, pp. 70–77, Feb. 2022, doi: 10.1109/MWC.007.00345.

[28] M. Yi, Y. Bae, S. Yoo, and J. So, "Digitized reconfigurable metal reflectarray surfaces for millimeter-wave beam-engineering," *Appl. Sci.*, vol. 11, no. 13, p. 5811, Jun. 2021, doi: 10.3390/app11135811.

[29] L. Wu, L. Wu, K. Lou, J. Ke, J. Liang, Z. Luo, J. Y. Dai, Q. Cheng, and T. J. Cui, "A wideband amplifying reconfigurable intelligent surface," *IEEE Trans. Antennas Propag.*, vol. 70, no. 11, pp. 10623–10631, Nov. 2022, doi: 10.1109/TAP.2022.3187137.

[30] M. Dajer, Z. Ma, L. Piazzi, N. Prasad, X.-F. Qi, B. Sheen, J. Yang, and G. Yue, "Reconfigurable intelligent surface: Design the channel—A new opportunity for future wireless networks," *Digit. Commun. Netw.*, vol. 8, no. 2, pp. 87–104, Apr. 2022, doi: 10.1016/j.dcan.2021.11.002.

[31] E. C. Strinati, G. C. Alexandropoulos, H. Wymeersch, B. Denis, V. Sciancalepore, R. D'Errico, A. Clemente, D.-T. Phan-Huy, E. De Carvalho, and P. Popovski, "Reconfigurable, intelligent, and sustainable wireless environments for 6G smart connectivity," *IEEE Commun. Mag.*, vol. 59, no. 10, pp. 99–105, Oct. 2021, doi: 10.1109/MCOM.001.2100070.

[32] P. Staat, S. Mulzer, S. Roth, V. Moonsamy, M. Heinrichs, R. Kronberger, A. Sezgin, and C. Paar, "IRShield: A countermeasure against adversarial physical-layer wireless sensing," in *Proc. IEEE Symp. Secur. Privacy (SP)*, May 2022, pp. 1705–1721, doi: 10.1109/SP46214.2022.9833676.

[33] O. Özdogan, E. Björnson, and E. G. Larsson, "Intelligent reflecting surfaces: Physics, propagation, and pathloss modeling," *IEEE Wireless Commun. Lett.*, vol. 9, no. 5, pp. 581–585, May 2020, doi: 10.1109/LWC.2019.2960779.

[34] V. Tapio, A. Shojaeifard, D. Jagyasi, P. Pirinen, and M. Juntti, "Coverage enhancements using RIS-integrated NR," in *Proc. IEEE Global Commun. Conf.*, Dec. 2022, pp. 2358–2362, doi: 10.1109/GLOBECOM48099.2022.10001290.

[35] C. K. Anjinappa, F. Erden, and I. Guvenc, "Base station and passive reflectors placement for urban mmWave networks," *IEEE Trans. Veh. Technol.*, vol. 70, no. 4, pp. 3525–3539, Apr. 2021, doi: 10.1109/TVT.2021.3065221.

[36] D. Solomitckii, C. B. Barneto, M. Turunen, M. Allen, G. P. Zhabko, S. V. Zavjalov, S. V. Volvenko, and M. Valkama, "Millimeter-wave radar scheme with passive reflector for uncontrolled blind urban intersection," *IEEE Trans. Veh. Technol.*, vol. 70, no. 8, pp. 7335–7346, Aug. 2021, doi: 10.1109/TVT.2021.3093822.

[37] H. Matsuno, T. Ohto, and T. Hayashi, "Development of intelligent reflecting surfaces for mobile communication systems," in *Proc. IEEE Int. Workshop Electromagn., Appl. Student Innov. Competition (iWEM)*, Narashino, Japan, Aug. 2022, pp. 5–6, doi: 10.1109/iWEM52897.2022.9993561.

[38] O. Ozdemir, F. Erden, I. Guvenc, T. Yekan, and T. Zarian, "28 GHz mmWave channel measurements: A comparison of horn and phased array antennas and coverage enhancement using passive and active repeaters," 2020, *arXiv:2002.00121*.

[39] E. Martinez-de Rioja, A. F. Vaquero, M. Arrebola, E. Carrasco, J. A. Encinar, and M. Achour, "Passive dual-polarized shaped-beam reflectarrays to improve coverage in millimeter-wave 5G networks," in *Proc. 15th Eur. Conf. Antennas Propag. (EuCAP)*, Düsseldorf, Germany, Mar. 2021, pp. 1–5, doi: 10.23919/EuCAP51087.2021.9411196.

[40] E. Carrasco, M. Barba, J. A. Encinar, M. Arrebola, F. Rossi, and A. Freni, "Design, manufacture and test of a low-cost shaped-beam reflectarray using a single layer of varying-sized printed dipoles," *IEEE Trans. Antennas Propag.*, vol. 61, no. 6, pp. 3077–3085, Jun. 2013, doi: 10.1109/TAP.2013.2254431.

[41] J. S. Romero-Peña and N. Cardona, "Irregular multifocal reflector for efficient mmWave propagation in indoor environments," in *Proc. 14th Eur. Conf. Antennas Propag. (EuCAP)*, Copenhagen, Denmark, Mar. 2020, pp. 1–5, doi: 10.23919/EuCAP48036.2020.9136074.

[42] C. K. Anjinappa, A. P. Ganesh, O. Ozdemir, K. Ridenour, W. Khawaja, I. Guvenc, H. Nomoto, and Y. Ide, "Indoor propagation measurements with transparent reflectors at 28/39/120/144 GHz," in *Proc. IEEE Int. Conf. Commun. Workshops*, May 2022, pp. 1118–1123, doi: 10.1109/ICCWorkshops53468.2022.9814550.

[43] X. Meng, M. Nekovee, and D. Wu, "The design and analysis of electronically reconfigurable liquid crystal-based reflectarray metasurface for 6G beamforming, beamsteering, and beamsplitting," *IEEE Access*, vol. 9, pp. 155564–155575, 2021, doi: 10.1109/ACCESS.2021.3125837.

[44] J. Chan, C. Zheng, and X. Zhou, "3D printing your wireless coverage," in *Proc. 2nd ACM Int. Workshop Hot Topics Wireless (HotWireless)*, Paris, France, Sep. 2015, pp. 1–5, doi: 10.1145/2799650.2799653.

[45] B. V. Ultimaker. *Ultimaker S5*. Accessed: Apr. 13, 2023. [Online]. Available: http://www.ultimaker.com/de/3d-printers/ultimaker-s5

[46] D. Betancourt, C. Galvis-Salzburg, and F. Weinmann, "Development and characterization of a plastic 3D-printed only external-layer metal-coated waveguide antenna array," in *Proc. 15th Eur. Conf. Antennas Propag. (EuCAP)*, Mar. 2021pp. 1–5, doi: 10.23919/EuCAP51087.2021.9411209.

[47] MG Chemicals Ltd. *843AR Super Shield Silver-Coated Copper Conductive Spray Paint*. Accessed: Apr. 13, 2023. [Online]. Available: http://www.mgchemicals.com/downloads/tds/tds-843ar-a.pdf

[48] K. Heimann, J. Tiemann, D. Yolchyan, and C. Wietfeld, "Experimental 5G mmWave beam tracking testbed for evaluation of vehicular communications," in *Proc. IEEE 2nd 5G World Forum (5GWF)*, Dresden, Germany, Sep. 2019, pp. 382–387, doi: 10.1109/5GWF.2019.8911692.

[49] X. Liu, L. Schmitt, B. Sievert, J. Lipka, C. Geng, K. Kolpatzeck, D. Erni, A. Rennings, J. C. Balzer, M. Hoffmann, and A. Czylwik, "Terahertz beam steering using a MEMS-based reflectarray configured by a genetic algorithm," *IEEE Access*, vol. 10, pp. 84458–84472, 2022, doi: 10.1109/ACCESS.2022.3197202.

[50] Z. Peng, L. Li, M. Wang, Z. Zhang, Q. Liu, Y. Liu, and R. Liu, "An effective coverage scheme with passive-reflectors for urban millimeter-wave communication," *IEEE Antennas Wireless Propag. Lett.*, vol. 15, pp. 398–401, 2016, doi: 10.1109/LAWP.2015.2447734.

[51] National Instruments Corp. (Nov. 2022). *Introduction to the NI mmWave Transceiver System Hardware*. Accessed: Apr. 13, 2023. [Online]. Available: http://www.ni.com/en/innovations/white-papers/16/introduction-to-the-ni-mmwave-transceiver-system-hardware.html

[52] F. Erden, O. Ozdemir, W. Khawaja, and I. Guvenc, "Correction of channel sounding clock drift and antenna rotation effects for mmWave angular profile measurements," *IEEE Open J. Antennas Propag.*, vol. 1, pp. 71–87, 2020, doi: 10.1109/OJAP.2020.2979243.

[53] G. Raney, B. Unruh, R. Lovestead, and B. Winther, "64-element 28 gigahertz phased array 5G prototyping platform," in *Proc. 11th Global Symp. Millim. Waves (GSMM)*, May 2018, pp. 1–4, doi: 10.1109/GSMM.2018.8439161.

[54] Infinite Electronics Inc. *WR-28 Waveguide Standard Gain Horn Antenna*. Accessed: Apr. 13, 2023-04-13. [Online]. Available: http://www.pasternack.com/images/ProductPDF/PE9850-2F-10.pdf

[55] *TSG RAN; UE Radio Transmission and Reception; Part 2: Range 2 Standalone (Release 17)*, 3GPP, document 38.101-2, Sep. 2022.

[56] Ansys Inc. *High Frequency Simulation Software (HFSS)*. Accessed: Apr. 13, 2023. [Online]. Available: http://www.ansys.com/hfss

[57] S. Hager, S. Bocker, S. Jamali, T. Reinsch, and C. Wietfeld, "A novel system architecture for small-scale motion sensing exploiting 5G mmWave channels," in *Proc. IEEE Globecom Workshops (GC Wkshps)*, Dec. 2021, pp. 1–6, doi: 10.1109/GCWkshps52748.2021.9682166.

[58] *Recommendation P.1238-7: Propagation Data and Prediction Methods for the Planning of Indoor Radiocommunication Systems and Radio Local Area Networks in the Frequency Range 900 MHz to 100 GHz*, International Telecommunication Union, Geneva, Switzerland, Feb. 2012.

[59] A. Roessler, "Pre-5G and 5G: Will the mmWave link work?" *Microwave J.*, vol. 60, no. 12, pp. 1–16, Dec. 2017.

[60] S. Kutty and D. Sen, "Beamforming for millimeter wave communications: An inclusive survey," *IEEE Commun. Surveys Tuts.*, vol. 18, no. 2, pp. 949–973, 4th Quart., 2016, doi: 10.1109/COMST.2015.2504600.

SIMON HÄGER (Student Member, IEEE) received the B.Sc. degree in electrical engineering from Paderborn University, Paderborn, Germany, in 2018, and the M.Sc. degree in communications engineering from RWTH Aachen University, Aachen, Germany, in 2020. He is currently pursuing the Dr.-Ing. degree with TU Dortmund University, Dortmund, Germany, in mobile cellular millimeter-wave communications requiring well-designed reflector-based connectivity enhancements and beam management procedures. His research with the Communication Networks Institute also focuses on the efficient provisioning of native channel-based sensing services with mmWave networks.

KARSTEN HEIMANN received the M.Sc. degree in electrical engineering and information technology from TU Dortmund University, Dortmund, Germany, in 2016. He is currently a Research Assistant with the Faculty of Electrical Engineering and Information Technology, Communication Networks Institute, TU Dortmund University. His research interests include wireless communications in cellular networks of 5G and beyond with a particular focus on the millimeter-wave domain.

STEFAN BÖCKER (Member, IEEE) received the Dipl.-Ing. degree from TU Dortmund University, Dortmund, Germany, in 2013. He started as a Research Assistant with the Faculty of Electrical Engineering and Information Technology, Communication Networks Institute (CNI), TU Dortmund University. In 2016, he took over as the Institute's Head of the Research Group for 5G networks before being appointed as the Chief Engineer, in 2021, where he is currently responsible for the coordination of third-party funded research activities. His research interests include scalability in unlicensed frequency domains, 5G networks with a focus on mMTC, and operation of private networks in licensed domains with a special interest in industrial IoT environments.

CHRISTIAN WIETFELD (Senior Member, IEEE) received the Dr.-Ing. and Dipl.-Ing. degrees from RWTH Aachen University, Aachen, Germany. He is currently a Full Professor and the Head of the Communication Networks Institute, TU Dortmund University, Dortmund, Germany. For more than 30 years, he has been a Coordinator and a Contributor to large-scale research projects on internet-based mobile communication systems within both academia and industry with RWTH Aachen (1992–1997), Siemens AG (1997–2005), and TU Dortmund (since 2005). His current research interests include the design and performance evaluation of 5G and 6G communication networks for cyber-physical systems in energy, transport, robotics, and emergency response. He is the author of more than 300 peer-reviewed papers and holds several patents. He has been a Co-Founder of the IEEE Global Communications Conference Workshop on Wireless Networking for Unmanned Autonomous Vehicles and a member of the Technical Editor Board of the *IEEE Wireless Communication Magazine*. In addition to more than ten IEEE best paper awards, he was a recipient of the ITU-T Outstanding Contribution Award for his work on the standardization of next-generation mobile network architectures.

• • •